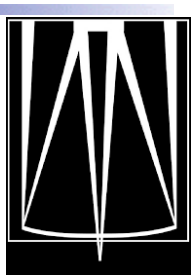

Vibration Measurements using ‘Alopeke

GNAO-SYS-SIM-010

Related PBS ID: 5.2

M. van Dam, A. Stephens, G. Sivo

September 23, 2020

Table of Contents

Document Acceptance and Release Notice
This document is a managed document. To identify changes, each page contains a release number and a page number. This document is authorized for release once all signatures have been obtained.

APPROVED:	*Approval on file* William Rambold GNAO Project Lead Systems Engineer	Date:	2020-11-12
APPROVED:	*Approval on file* Manuel Lazo GNAO Project Manager	Date:	2020-11-12
APPROVED:	*Approval on file* Gaetano Sivo GNAO Principal Investigator	Date:	2020-11-12
APPROVED:	*Approval on file* Henry Roe GNAO Sponsor, Gemini Deputy Director	Date:	2020-11-12

Change Record

Version	Date	Description	Owner Name	Change Request
1.0	2020-11-12	Released through formal change control process	M. van Dam	GEM-192

1 Introduction

It is well known that Altair suffers from vibrations, and this limits the image quality even in ideal atmospheric conditions. The vibrations have a number of different sources, but it is believed that both Altair and GNIRS produce significant contributions. In order for GNAO to realize its scientific potential, we need to restrict the image quality degradation due to vibrations, which in turn requires us to understand the telescope environment.

In GNAO-SYS-SIM-008,[1] we show that we can use 'Alopeke to measure vibrations on the Gemini North telescope. These measurements, made in August 2020 during twilight, and are the subject of the current report.

2 Telescope and instrument configuration

A number of measurements were taken over different nights with a different setup. In all cases, the data was captured using the blue channel using the wide plate scale (72.5 mas) in 4x4 binning, for a total plate scale of 290 mas.

The important telescope and instrument parameters are tabulated in Table 1. The kinetic cycle time (KCT) is the time between successive frames, which is essentially the frame rate. Note that the exposure time is significantly shorter than the KCT. For example, a KCT of 1.942 ms consists of an integration time of 1.320 ms.

The Cass Rotator position angle (CRPA) describes the orientation of the Cass Rotator.

In much of the data, guiding was enabled using PWFS2 running at 200 Hz with a PID controller. The 0 dB control bandwidth is believed to be 20 Hz, so it clearly impacts on the measurements: low frequencies are corrected, mid-range frequencies are amplified and tip-tilt anisoplanatism (also known as anisokinetism) is introduced due to the fact that PWFS2 is so far off-axis.

VTK is a vibration rejection algorithm designed to strongly reject 12 Hz vibration. In any event, the data did not show a strong 12 Hz vibration even when the PWFS2 was not running.

[1] Marcos van Dam, Gaetano Sivo and Andrew Stephens, "Impact of Telescope Vibrations on GNAO Performance," GNAO-SYS-SIM-008 v1.0 15 July 2020.

File	KCT	Azimuth	Elevation	CRPA	Guiding	VTK
N20200804A0175b	0.001942	331.96	64.99	36.389	On	On
N20200804A0176b	0.002042	254.81	56.95	203.305	On	On
N20200804A0177b	0.003443	252.88	59.22	114.55	On	On
N20200808A0001b	0.001942	301.16	64.48	70.225	On	On
N20200808A0002b	0.001942	299.74	62.6	117.68	On	On
N20200808A0003b	0.001942	299.14	61.67	163.786	On	On
N20200808A0004b	0.001942	298.7	60.91	209.636	On	On
N20200808A0005b	0.001942	298.23	60.02	255.604	On	On
N20200808A0006b	0.001942	297.55	58.62	-57.954	Off	On
N20200809A0288b	0.001942	14.19	70.32	-16.653	On	Off
N20200809A0289b	0.001942	13.64	70.37	-15.981	On	Off
N20200809A0290b	0.001942	11.91	70.53	31.132	On	Off
N20200809A0291b	0.001942	10.34	70.65	78.045	On	Off
N20200809A0292b	0.001942	7.22	70.83	126.845	On	Off
N20200809A0293b	0.001942	5.49	70.9	173.954	On	Off
N20200809A0294b	0.001942	4.11	70.95	220.635	On	Off
N20200809A0295b	0.001942	0.42	71.01	-89.913	On	Off
N20200809A0296b	0.001942	-0.44	71.01	-88.875	Off	Off
N20200810A0505b	0.001942	43.79	82.33	-45.12	On	Off
N20200810A0506b	0.001942	37.33	83.08	-83.019	On	Off
N20200810A0507b	0.001942	24.59	83.98	-114.246	Off	Off
N20200810A0508b	0.001942	17.8	84.25	-151.991	Off	Off
N20200810A0509b	0.001942	11.49	84.42	-190.372	Off	Off
N20200811A0002b	0.001942	277.42	65.55	91.949	On	On
N20200811A0003b	0.001942	277.44	65.24	92.043	On	Off
N20200811A0004b	0.001942	277.58	64.19	-87.676	On	On
N20200811A0005b	0.001942	277.61	63.9	-87.589	On	Off
N20200811A0006b	0.001942	277.68	62.93	2.721	On	On
N20200811A0007b	0.001942	277.73	62.47	2.854	On	Off

Table 1: Configurations used for making the measurements

The instruments installed on the telescope are shown in Table 2. In the future, data will be taken with GNIRS cooling turned off to measure the difference.

Port	1	2	3	4	5
Instrument	NIRI	Alopeke/GCAL	GNIRS	Altair	GMOS

Table 2: Instruments installed on the telescope

3 Analysis

The data sets consist of 30 000 consecutive frames of data, which consists of almost one minute of data at a frame rate of 514.6 Hz. The first five frames are typically bad and are removed from consideration. Figure 1 shows typical speckles and their temporal evolution.

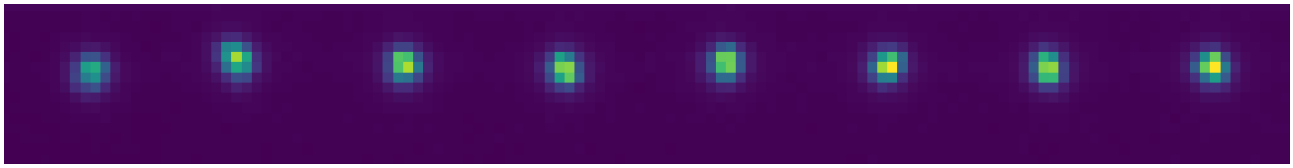

Figure 1: Speckles taken approximately two seconds apart

The centroid of the speckle images is extracted using the correlation algorithm which operates as follows. A 2D Gaussian reference image is created with a FWHM slightly larger than the images. The cross-correlation between the reference image and the speckle image is found, and the maximum value is obtained using quadratic interpolation. The centroid is multiplied by the plate scale of the binned pixels to obtain the displacement of the spot in milliarcseconds. The average x- and y-centroid value is removed, since it is not meaningful.

The time series of the centroid data is converted to the Fourier domain in order to understand the frequencies of the vibrations. In order to reduce the noise in the data, we first split the time series into 16 shorter time series. A Hanning window is applied to each set of data to reduce the effect of spectral leakage and the Fourier transform is obtained. The power spectral density is converted to a single-sided power spectrum and normalized to have units of mas^2/Hz. This is useful because the sets are not all taken at the same frame rate.

As an example, let us consider the first data set, N20200804A0175b. The spots are tightly distributed near the center, as shown in Figure 2.

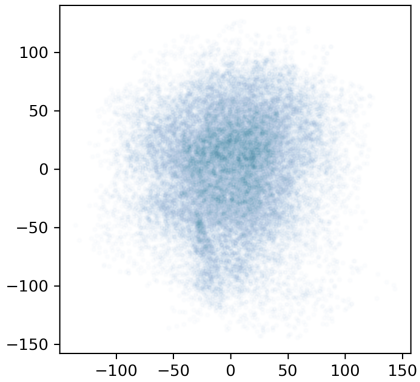

Figure 2: Position of centroid (mas) over the data set N20200804A0175b.

The power spectral density is displayed in Figure 3. The square of the open-loop centroid error is given by the area under the curve of the linear plot. This is mostly low frequencies (<3 Hz) as well as a small number of vibration spikes. However, the higher frequencies are more important when we consider the effect of closed-loop control.

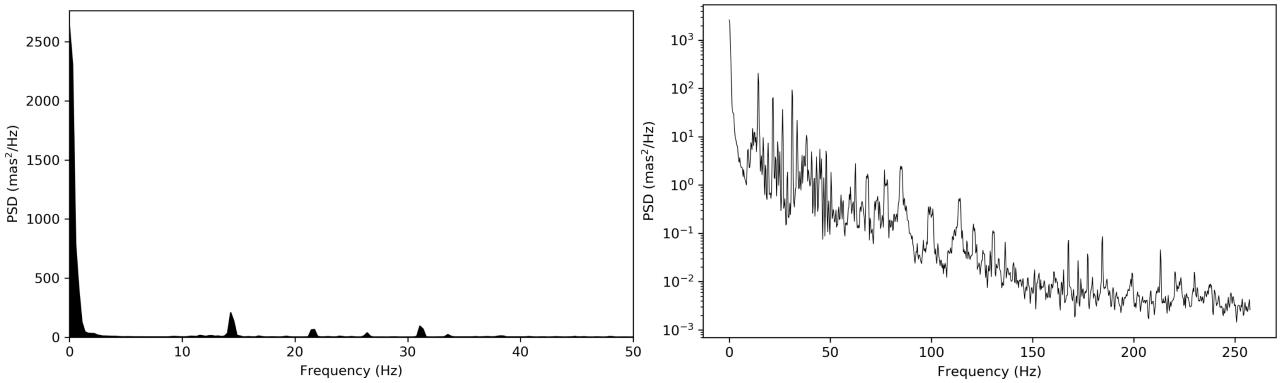

Figure 3: Power spectral density as a function of frequency using a linear (left) and logarithmic (right) y-scale.

The data above shows a conspicuous absence of a spike at 12 Hz. Looking at the power spectrum of the data without averaging (in order to get the highest possible spectral resolution), we find that there is indeed a spike at exactly 12 Hz, but it is not very large, as shown in Figure 4.

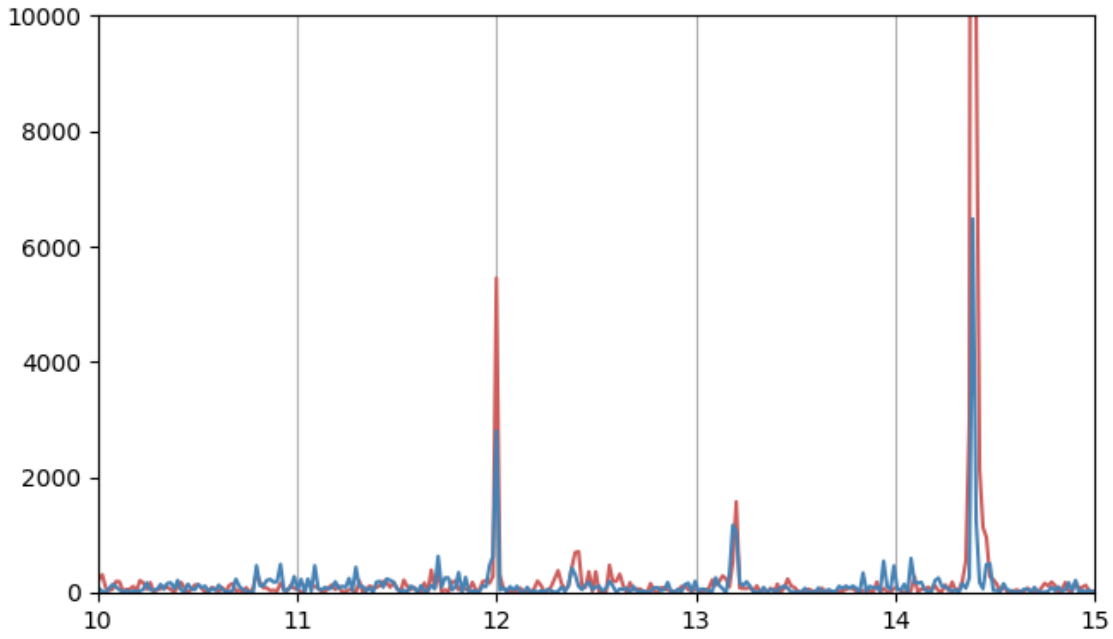

Figure 4: Power spectrum of x- (red) and y-centroids (blue) for N20200808A0006b.fits, which had the guiding turned off. The units for the y-axis are arbitrary.

For the purposes of this study, we will consider the controller to be a closed-loop integrator with a variable loop gain, set to 0.3. The loop delay is set to one frame, and the dynamics of the tip-tilt mirror are ignored. The method used to compute the rejection transfer function is described in van Dam *et al*.[2] The rejection transfer function is shown in Figure 5. The disturbances at low frequencies are well corrected, but above 40 Hz, the correction makes things worse.

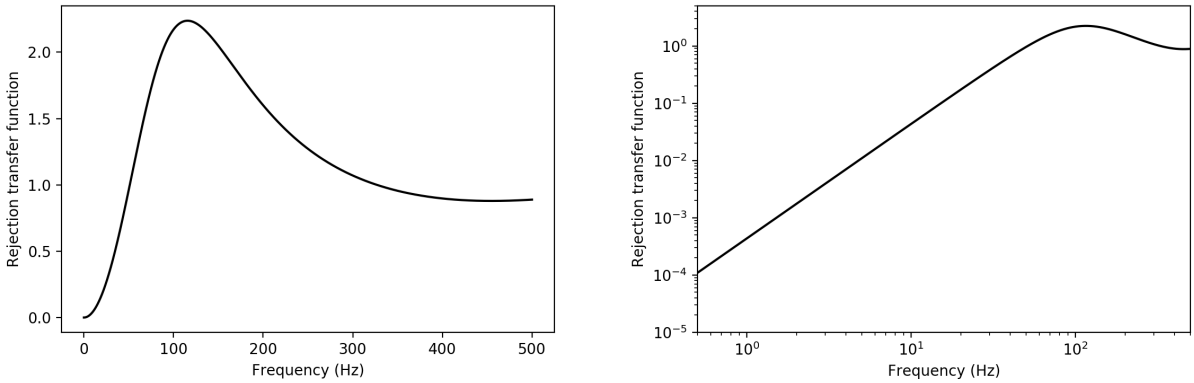

Figure 5: Rejection transfer function for the tip-tilt controller running at 1 kHz on a linear scale (left) and a log-log scale (right).

4 Results

There are different conventions about how to report tip-tilt. In this report, and following on from work on the GNAO simulations, we define a tip-tilt angle-of-arrival value to be the average of the x- and y-values in quadrature:

[2]van Dam, Marcos A., David Le Mignant, and Bruce A. Macintosh. "Performance of the Keck Observatory adaptive-optics system." Applied Optics 43.29 (2004): 5458-5467.

$$\sigma_{TT} = \sqrt{(\sigma_X^2 + \sigma_Y^2)/2} \quad (1)$$

The results of the 29 data sets in Table 1 were analyzed. Figure 6 shows the residual tip-tilt error after correction by a tip-tilt controller running at 500 Hz with a loop gain of 0.3, which is the typical case expected when guiding on moderately bright tip-tilt stars. The performance is better (or, at least, no worse) when the guiding is disabled. This is to be expected, since the guider is injecting frequencies that the tip-tilt controller cannot correct. In the analysis that follows, we do not differentiate between data sets taken with guiding on and off. However, all future data should be taken with guiding at a reduced frequency of 20 Hz in order to avoid compensating the frequencies of interest.

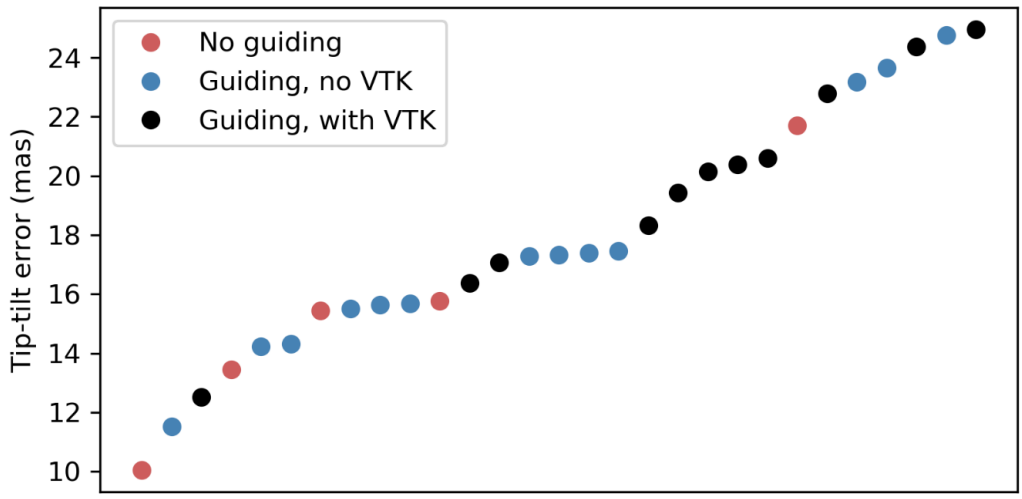

Figure 6: Residual tip-tilt following tip-tilt correction at 500 Hz. The values are sorted in ascending order.

Figure 7 plots the residual tip-tilt as a function of frame rate for typical frame rates. There is a significant increase in tip-tilt error as the frame rate is reduced.

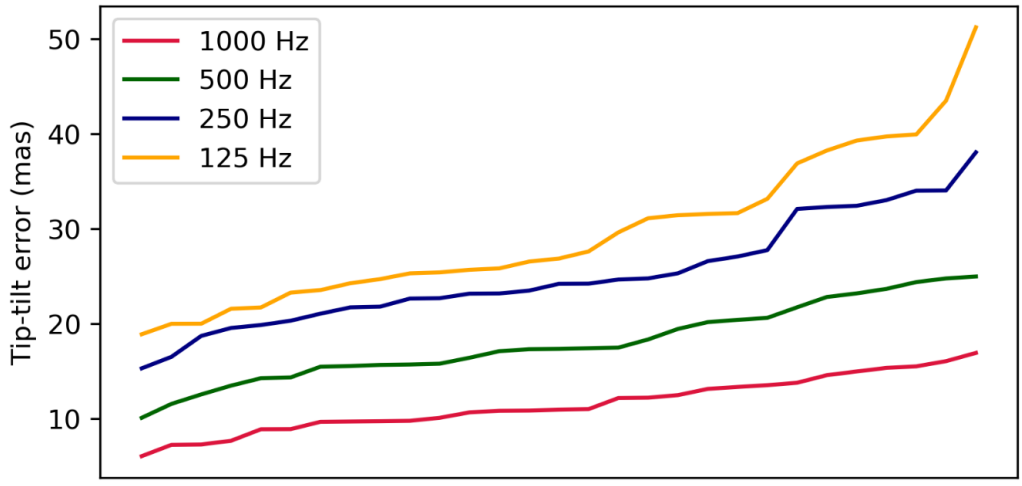

Figure 7: Residual tip-tilt as a function of controller frame rate. The values are sorted in ascending order.

The performance as a function of elevation is shown in Figure 8. It appears that the performance is has a non-linear dependence on elevation, but more data is needed to understand this better. No dependence on azimuth of CRPA was evident from the data.

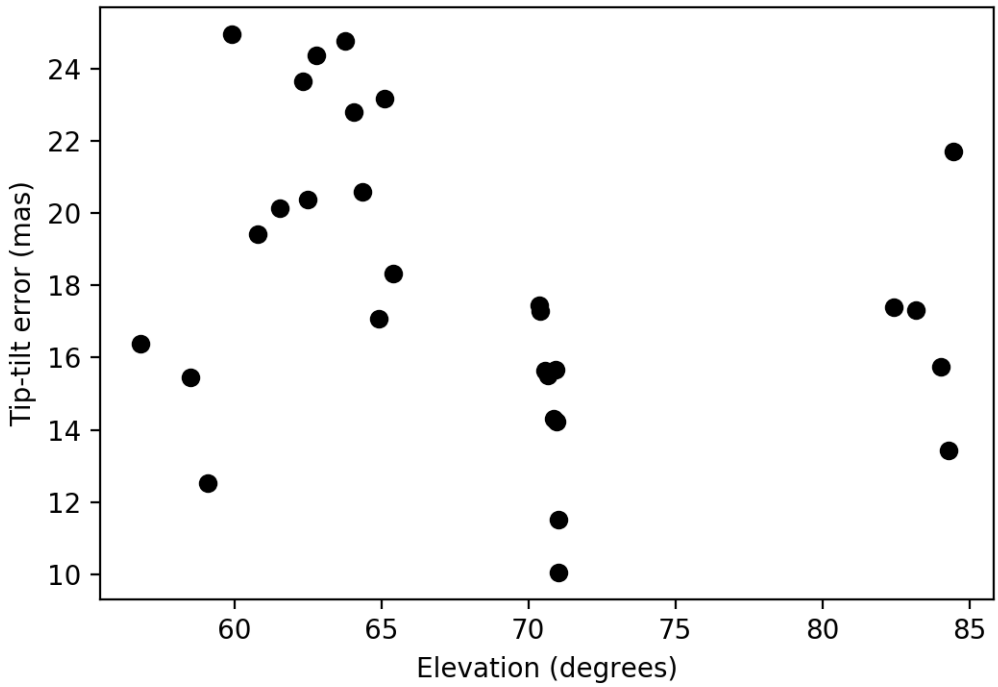

Figure 8: Residual tip-tilt as a function of elevation for a tip-tilt controller running at 500 Hz.

A dedicated experiment was subsequently performed to compare the results as a function of elevation. The results, tabulated in Table 3, show that the magnitude of the residual tip-tilt does not depend on elevation.

Elevation	33°	33°	41°	71°	84°
Residual tip-tilt at 500 Hz (mas)	19.6	19.6	19.9	20.2	19.3

Table 3:Residual tip-tilt when compensated at 500 Hz as a function of elevation.

The FWHM was estimated from the median value of the short exposure images. The FWHM calculation overestimates the seeing and is very approximate because the spots are undersampled. There is no obvious relationship between seeing and tip-tilt error, as seen in Figure 9.

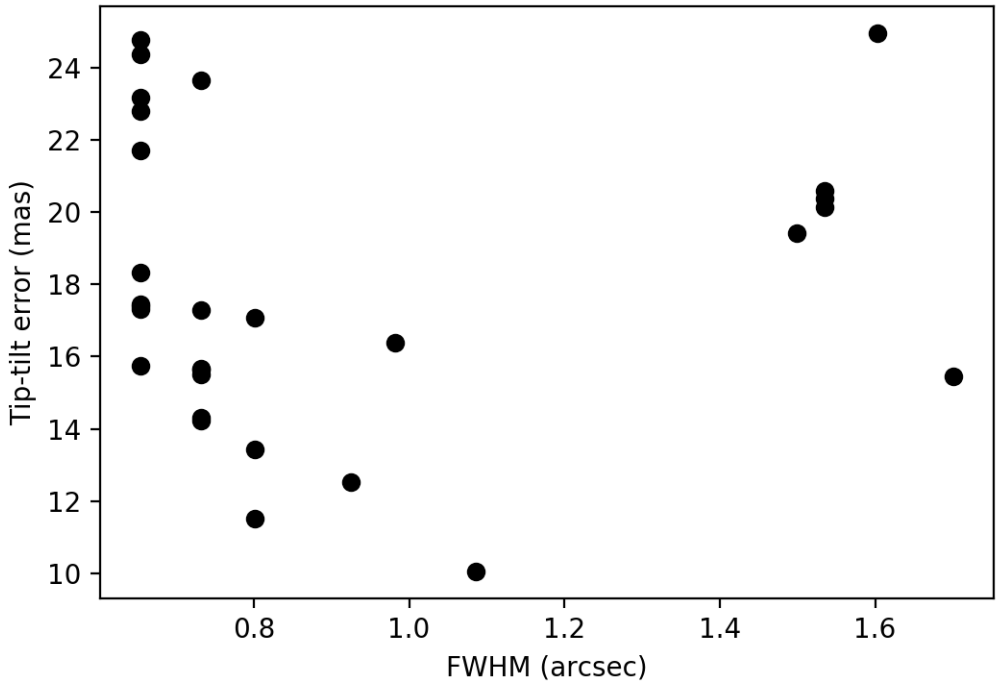

Figure 9: Residual tip-tilt as a function of FWHM for a tip-tilt controller running at 500 Hz.

Let us consider the residual tip-tilt error at 500 Hz for the five no guiding cases (five red dots on Figure 6) to see what frequencies are dominant. The power spectra with the same axes are plotted in Figure 10. The plots show the energy of the vibration peaks spread over a wider range of frequencies due to the averaging of the power spectra. All of the data shows a forest of lines, and in some cases there is also broad lumps in the regions between 14-18 Hz and 36-44 Hz. It is possible to use controllers that cancel the vibration peaks.

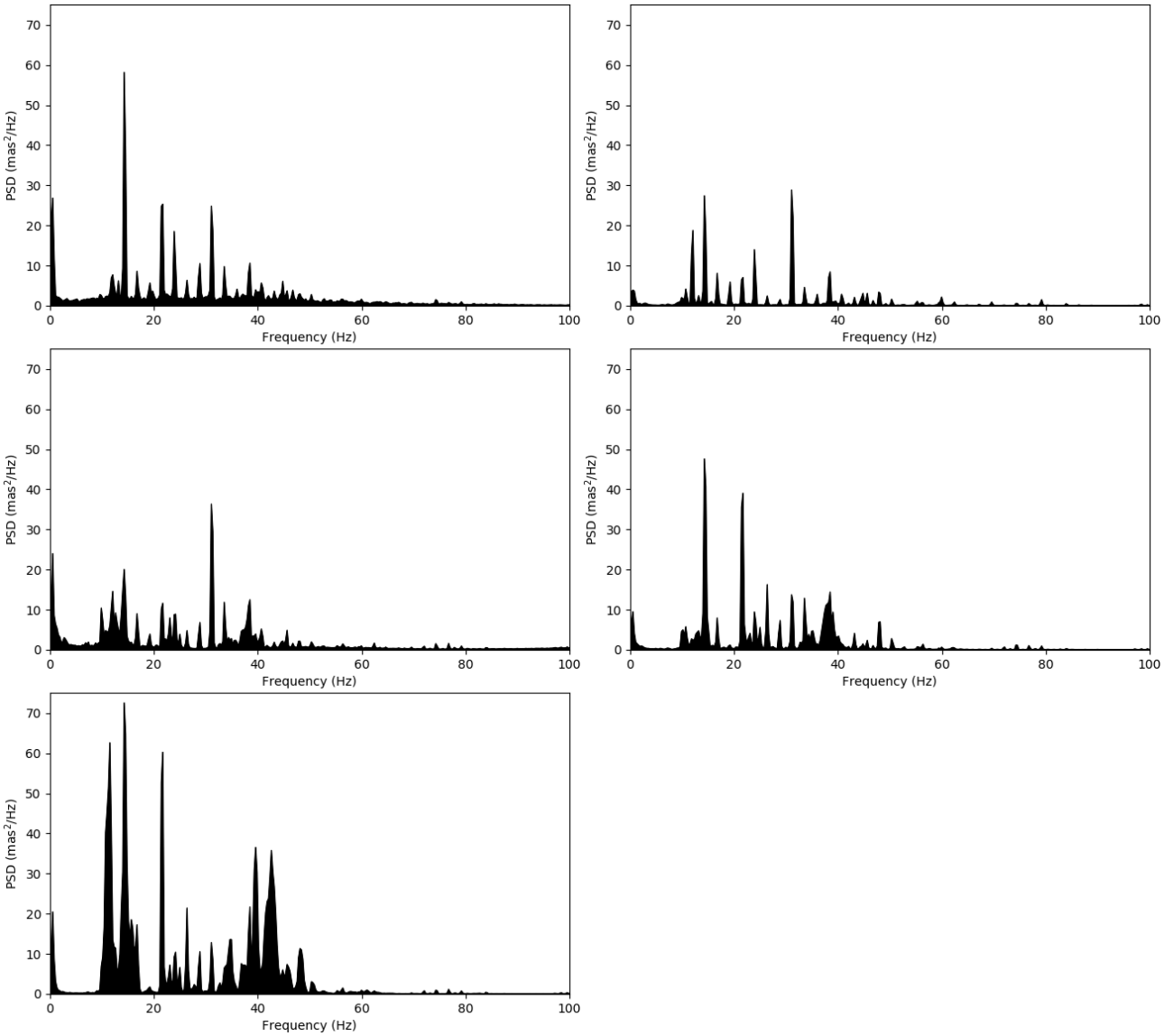

Figure 10: Power spectral density of the residual error after correction at 500 Hz. The axes are the same in all cases.

It is commonly believed that observing with GNIRS mounted and pumping with the CRPA at 90° or -90° shakes the M1 cell and produces vibrations at 12.0 Hz. Additional data was taken on 21 September 2020 to understand the how the CRPA affects vibrations. This data was taken with the guider operating at the reduced frequency of 20 Hz with no VTK correction.

Table 4 shows the CRPA values, the power at 12 Hz (integrated between 11.7 Hz and 12.3 Hz, but consisting mostly of a narrow peak at exactly 12 Hz), the residual tip-tilt when compensated at 500 Hz. There is weak evidence to suggest that the vibrations are worse when the CRPA is at 180°, and not at 90° and at 270°.

CRPA	90°	120°	150°	180°	210°	240°
Uncompensated 12 Hz vibration	6650	5620	2600	1565	3006	14300
Residual tip-tilt at 500 Hz (mas)	13.7	14.8	14.7	19.3	18.5	15.6

Table 4: Uncompensated 12 Hz vibration and total residual tip-tilt when compensated at 500 Hz.

5 Controllers

The analysis of the residual tip-tilt was carried out using a simple control law typical of what is used in most tip-tilt controllers: an integrator with a loop gain of 0.3. The transfer function is

$$H(z) = \frac{0.3}{1 + z^{-1}} \tag{2}$$

More sophisticated controllers are possible. A notch filter could be used to reject narrow vibration spikes, but the "forest" of lines in the power spectrum makes this approach complicated. Instead, we could consider a controller with better rejection over the frequencies of interest.

The data was reanalyzed using a double integrator with a lead-lag compensator. Its transfer function is

$$H(z) = \frac{1.665 - 4.148z^{-1} + 3.904z^{-2} - 1.675z^{-3} + 0.262z^{-4}}{1 - 2.065z^{-1} + 1.306z^{-2} - 0.413z^{-3} + 0.172z^{-4}} \tag{3}$$

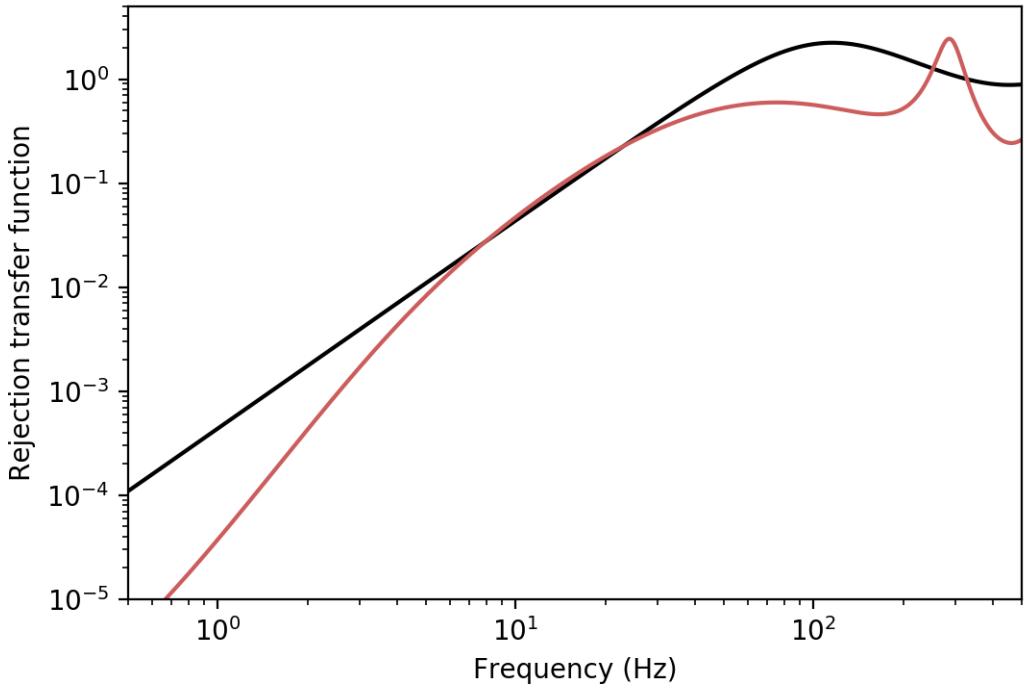

Figure 11: Rejection transfer function for an integrator (black) and a double integrator with a lead-lag compensator (red).

The double integrator has better rejection at all of the frequencies of interest, but adds passes a factor of 2.45 times more noise to the tip-tilt mirror. Reanalyzing the CRPA data set at 500 Hz and 1000 Hz with both types of controller shows that optimizing the shape of the rejection is a promising avenue for future research (Table 5).

CRPA		90°	120°	150°	180°	210°	240°
Integrator	500 Hz	13.7	14.8	14.7	19.3	18.5	15.6
Integrator	1000 Hz	8.9	9.7	9.6	12.9	12.1	10.0
Double Integrator	500 Hz	9.7	10.5	10.5	13.4	12.8	10.7
Double Integrator	1000 Hz	7.1	7.6	7.6	9.9	9.5	7.9

Table 5: Residual tip-tilt compensated with an integrator and with a double integrator and a lead-lag compensator at 500 Hz and 1000 Hz.

6 Conclusion

In this report, we present the results of vibration measurements made using ‘Alopeke. The results are consistent with what we expected based on tip-tilt measurements made with Altair. The power spectrum exhibits power over a wide range of frequencies, including a large number of very narrow lines. Although we measure a narrow line at 12 Hz, this represents a very small fraction of the disturbances.

In order to limit the reduction in K-band to 10% or less, we need to keep the tip-tilt error to less than 8.25 mas. If we use a tip-tilt controller running at 500 Hz with a loop gain of 0.3, we find that the residual tip-tilt lies in the range between 10 mas and 24 mas, which exceeds the allowable values. It is possible to achieve tip-tilt residuals of 7 mas to 10 mas by running a sophisticated controller at 1000 Hz. This would only work when guiding on a very bright star in order to keep the measurement noise sufficiently low.

Remediation work on the telescope should focus on vibrations in the 10 Hz to 50 Hz range, which have the largest impact on the adaptive optics system. In addition, we should investigate the use of controllers that have good rejection over this region.